



Contents lists available at ScienceDirect

## Journal of Pharmaceutical Analysis

journal homepage: [www.elsevier.com/locate/jpa](http://www.elsevier.com/locate/jpa)

## Original article

# Identification of potential anti-pneumonia pharmacological components of *Glycyrrhizae Radix et Rhizoma* after the treatment with Gan An He Ji oral liquid

Xiaojuan Jiang<sup>a,1</sup>, Yihua Lin<sup>b,c,1</sup>, Yunlong Wu<sup>a</sup>, Caixia Yuan<sup>a</sup>, Xuli Lang<sup>a</sup>, Jiayun Chen<sup>a</sup>, Chunyan Zhu<sup>a</sup>, Xinyi Yang<sup>d</sup>, Yu Huang<sup>e</sup>, Hao Wang<sup>f,g,h,\*\*</sup>, Caisheng Wu<sup>a,\*</sup>

<sup>a</sup> Fujian Provincial Key Laboratory of Innovative Drug Target Research and State Key Laboratory of Cell Stress Biology, School of Pharmaceutical Sciences, Xiamen University, Xiamen, Fujian, 361102, China

<sup>b</sup> Department of Respiratory and Critical Care Medicine, The Third Clinical Medical College, Fujian Medical University, Fuzhou, 350122, China

<sup>c</sup> Department of Respiratory and Critical Care Medicine, The First Affiliated Hospital of Xiamen University, Xiamen, Fujian, 361003, China

<sup>d</sup> Laboratory of Pharmacology/Beijing Key Laboratory of Antimicrobial Agents, Institute of Medicinal Biotechnology, Chinese Academy of Medical Sciences and Peking Union Medical College, Beijing, 100050, China

<sup>e</sup> School of Pharmacy, Ningxia Medical University, Yinchuan, 750004, China

<sup>f</sup> School of Pharmacy, Minzu University of China, Beijing, 100081, China

<sup>g</sup> Key Laboratory of Ethnomedicine (Minzu University of China), Ministry of Education, Beijing, 100081, China

<sup>h</sup> Institute of National Security, Minzu University of China, Beijing, 100081, China

## ARTICLE INFO

## Article history:

Received 22 February 2022

Received in revised form

16 July 2022

Accepted 20 July 2022

Available online 5 August 2022

## Keywords:

*Glycyrrhizae Radix et Rhizoma*

Pneumonia

Active components

Inducible nitric oxide synthase

Glycyrrhetic acid

## ABSTRACT

*Glycyrrhizae Radix et Rhizoma*, a traditional Chinese medicine also known as Gan Cao (GC), is frequently included in clinical prescriptions for the treatment of pneumonia. However, the pharmacological components of GC for pneumonia treatment are rarely explored. Gan An He Ji oral liquid (GAHJ) has a simple composition and contains GC liquid extracts and paregoric, and has been used clinically for many years. Therefore, GAHJ was selected as a compound preparation for the study of GC in the treatment of pneumonia. We conducted an in vivo study of patients with pneumonia undergoing GAHJ treatments for three days. Using the intelligent mass spectrometry data-processing technologies to analyze the metabolism of GC in vivo, we obtained 168 related components of GC in humans, consisting of 24 prototype components and 144 metabolites, with 135 compounds screened in plasma and 82 in urine. After analysis of the metabolic transformation relationship and relative exposure, six components (liquiritin, liquiritigenin, glycyrrhizin, glycyrrhetic acid, daidzin, and formononetin) were selected as potential effective components. The experimental results based on two animal pneumonia models and the inflammatory cell model showed that the mixture of these six components was effective in the treatment of pneumonia and lung injury and could effectively downregulate the level of inducible nitric oxide synthase (iNOS). Interestingly, glycyrrhetic acid exhibited the strongest inhibition on iNOS and the highest exposure in vivo. The following molecular dynamic simulations indicated a strong bond between glycyrrhetic acid and iNOS. Thus, the current study provides a pharmaceutical basis for GC and reveals the possible corresponding mechanisms in pneumonia treatment.

© 2022 The Authors. Published by Elsevier B.V. on behalf of Xi'an Jiaotong University. This is an open access article under the CC BY-NC-ND license (<http://creativecommons.org/licenses/by-nc-nd/4.0/>).

Peer review under responsibility of Xi'an Jiaotong University.

\* Corresponding author.

\*\* Corresponding author. School of Pharmacy, Minzu University of China, Beijing, 100081, China.

E-mail addresses: [hao.wang@muc.edu.cn](mailto:hao.wang@muc.edu.cn) (H. Wang), [wucsh@xmu.edu.cn](mailto:wucsh@xmu.edu.cn) (C. Wu).

<sup>1</sup> Both authors contributed equally to this work.

<https://doi.org/10.1016/j.jpha.2022.07.004>

2095-1779/© 2022 The Authors. Published by Elsevier B.V. on behalf of Xi'an Jiaotong University. This is an open access article under the CC BY-NC-ND license (<http://creativecommons.org/licenses/by-nc-nd/4.0/>).

## 1. Introduction

*Glycyrrhizae Radix et Rhizoma*, also known as Gan Cao (GC), is a traditional Chinese medicine (TCM) material primarily derived from *Glycyrrhiza* species, i.e., the roots of *Glycyrrhiza inflata* Bat., *Glycyrrhiza glabra* L., and *Glycyrrhiza uralensis* Fisch. [1–3]. It has been extensively applied in TCM clinical prescriptions. According to previous reports, approximately 60% of TCM prescriptions issued in

clinical practices contain GC [1,3]. Owing to its anti-bacterial, anti-inflammatory, anti-tumor, and anti-viral pharmacological activities [4–7], GC has been clinically utilized for treatment of cough, bronchitis, peptic ulcer, dermatitis [8–11], etc. Since the outbreak of coronavirus disease 2019, GC has been proven to be effective in a number of TCM formulas [12,13], such as the Qingfei Paidu decoction, Huashi Baidu prescription, Xuanfei Baidu prescription, and Lianhua Qingwen capsule [14–17]. The existing reports on pneumonia treatment with GC mainly focus on either its overall pharmacological actions or the mechanism of specific targets on its main monomer components. As a typical example, glycyrrhizin can suppress the reproduction of severe acute respiratory syndrome coronavirus 2 owing to its angiotensin-converting enzyme 2 receptor-targeting capability [18]. However, the study of *in vivo* exposure compositions or effective medical components of GC that are efficacious in the treatment of respiratory diseases (e.g., pneumonia) remains to be performed.

Hundreds of species of Chinese herbal medicinal ingredients have “multi-components, multi-targets, and multi-functions” therapeutic effects [19]. The complexity of TCM causes difficulty in the investigation of effective medical components and their molecular mechanisms. At present, most TCMs are administered orally. Except some components of TCM that play roles in the regulation of the intestinal flora, most of the active components of TCM are mainly prototypes or related metabolites that can be absorbed under certain exposure *in vivo*. Therefore, through actual clinical human exposure, the efficiency of TCM active ingredient screening can be improved to a certain extent [20–22].

To identify the effective medicinal components of GC for pneumonia treatment, the current study aimed to comprehensively discover and identify GC-related components *in vivo* among patients with pneumonia after drug medication using ultra-high performance liquid chromatography-high-resolution mass spectrometry (UPLC-HRMS) and intelligent mass spectrometry (MS) data mining technology.

To meet the ethical requirements for human trials, we only considered commercial TCM formulas that contain GC as the main component and have been approved as suitable for the treatment of respiratory inflammations by the National Medical Products Administration (Beijing, China) for this study. Gan An He Ji oral liquid (GAHJ) was selected as the typical prescription in this study. Composed of GC liquid extract and paregoric, GAHJ relieves cough and breaks down phlegm. Clinically, it has been used for the treatment of patients with different types of pneumonia and has achieved satisfactory clinical outcomes. Given the simple compositions of GAHJ, it can effectively avoid the influence of other components on metabolic studies and further promote the discovery of potentially active GC components in patients with pneumonia.

Thus, the current study primarily aimed to comprehensively explore the *in vivo* exposure of GC and its potential effective medicinal components based on the intelligent MS data mining technology and exposure or metabolic pathways. The absorption, distribution, metabolism, and excretion (ADME) metabolic profiling analyses were also conducted on the relevant compositions of GC in rats to gain a deep understanding of the metabolic clearance process of the main GC substances exposed in the human body. In terms of action mechanisms, the potential effective medicinal components were selected as the research objects from an *in vivo* perspective. Furthermore, a network diagram was depicted for the “compound, disease, and target” relationship-based network pharmacological study to systematically analyze their inner links. Molecular modeling was then performed to predict the potential target proteins. Finally, systematic target and pharmacological validations were carried out

at different levels (e.g., cellular and pneumonia animal models) to verify the potential pharmaceutical basis of GAHJ in pneumonia treatment.

## 2. Methods and materials

### 2.1. Chemicals and materials

The following chemicals and materials were used: magnoflorine, liquiritin, ononin, daidzein, liquiritigenin, calycosin, formononetin, isoliquiritigenin, glycyrrhizin, and glycyrrhetic acid (purity  $\geq 98\%$ ; Baoji Chengguang Biological Co., Ltd., Baoji, China); blank Sprague-Dawley (SD) rat plasma (Shanghai Yuanye Biotechnology Co., Ltd., Shanghai, China); Oasis<sup>®</sup> hydrophilic lipophilic balance (HLB) solid-phase extraction column (6 mL/500 mg; Waters, Milford, MA, USA); methanol and acetonitrile (HPLC grade; Tedia High-Purity Solvents, Fairfield, OH, USA); formic acid (LCMS/HPLC grade; Anaqua<sup>™</sup> Chemicals Supply, Wilmington, DE, USA); normal saline (ChenXin Biology Co., Ltd., Jining, China); heparin sodium (Shanghai Aladdin Bio-Chem Technology Co., Ltd., Shanghai, China); lipopolysaccharide (LPS) (Beijing Solarbio Science & Technology Co., Ltd., Beijing, China); anti-inducible nitric oxide synthase (iNOS) antibody and tumor necrosis factor (TNF) receptor II (Abcam, Cambridge, UK); mouse iNOS enzyme-linked immunosorbent assay (ELISA) kit and mouse TNF- $\alpha$  ELISA kit (Wuhan Fine Test Biotech Co., Ltd., Wuhan, China); Hieff<sup>®</sup> quantitative polymerase chain reaction (qPCR) SYBR Green Master Mix (Low Rox Plus), Hifair<sup>®</sup> II 1st Strand cDNA Synthesis SuperMix for qPCR (gDNA digester plus), TRLeasy<sup>™</sup> Total RNA Extraction Reagent (Yeasen Biotechnology (Shanghai) Co., Ltd., Shanghai, China); polyacrylamide gel electrophoresis (PAGE) gel quick preparation kit (10%) (Suzhou NCM Biotech Co., Ltd., Suzhou, China); protease inhibitor cocktail (MedChemExpress, Monmouth Junction, NJ, USA); iNOS rabbit polyclonal antibody, 10–180 kDa protein marker (Wuhan ABclonal Biotechnology Co., Ltd., Wuhan, China); 1400W (Selleck, Shanghai, China); and ultrapure water preparation (Milli-Q water purification system, Merck KGaA, Darmstadt, Germany).

### 2.2. Collection of clinical samples

The clinical research protocol of this study was approved by the Medical Ethics Committee of the First Affiliated Hospital of Xiamen University (Ethics Review Approval No.: [2020] Scientific Research Ethics Review [053]; Xiamen, China). The current study was a single-center, randomized, and open-label clinical trial, with the enrollment of three male patients with pneumonia. All the patients provided a written informed consent before the enrollment. The sample collection process is detailed in Section 1 “Collection of clinical samples” in the Supplementary data.

### 2.3. Animal experiments

Male SD rats weighing 200–220 g and C57BL/6 mice weighing 18–20 g were used in the animal experiments. They were bought from the Laboratory Animal Center, Xiamen University (Xiamen, China). All animal care and experimental procedures were approved by the Animal Ethics Committee of Xiamen University (Animal Ethics Approval No.: XMULAC20210116). The animal adaptive feeding process is detailed in Section 2 “Animal experiments” in the Supplementary data.

#### 2.3.1. Drug administration and sample collection in rats

GAHJ was administered to the rats ( $n = 6$ ) intragastrically at 20 mL/kg. Three rats were placed in a metabolic cage, with blood samples collected from the fundus oculi venous plexus to collect a

blank plasma before administration and blank urine and fecal samples 12 h before the administration. The rats were administered with GAHJ once daily. After continuous administration for 7 days, sampling, including those for the blood, urine, and fecal samples, was performed on the three rats. In addition, the other three rats were used for bile sample collection. The drug administration and sample collection process are detailed in Section 2.1 “Collection of plasma, urine, and feces samples” and Section 2.2 “Collection of bile samples” in the Supplementary data.

### 2.3.2. Pneumonia model establishment and sample collection

**2.3.2.1. LPS-induced mouse model of pneumonia.** The mice were randomly divided into four groups: control (CON), model (LPS), pharmacodynamic component treatment (LPS-Mix), and GAHJ treatment (LPS-GAHJ) groups (with 10 mice in each group). The model was constructed by the nasal drip of LPS at 50  $\mu$ L per mouse. The grouping details were as follows: normal lung mice (CON); 10 mg/kg LPS-induced pneumonia mice treated with normal saline (LPS) [23,24]; 10 mg/kg LPS-induced pneumonia mice treated with 0.3 mL of pharmacodynamic component (LPS-Mix); and 10 mg/kg LPS-induced pneumonia mice treated with 0.3 mL of GAHJ (LPS-GAHJ). After inducement with LPS for 24 h, the mice were given drug treatment every 24 h for 7 days. Serum samples and lung tissues were collected on day 8.

**2.3.2.2. Staphylococcus aureus (S. aureus)-induced mouse model of pneumonia.** The mice were randomly divided into four groups, namely, control (CON), model (*S. aureus*), pharmacodynamic component treatment (*S. aureus*-Mix), and GAHJ treatment (*S. aureus*-GAHJ) groups, with 10 mice in each group. The model was constructed by the nasal drip of *S. aureus* (optical density of 0.1 at 600 nm) at 50  $\mu$ L per mouse [25]. The specific grouping information was the same as that of the LPS model.

## 2.4. Sample preparation

### 2.4.1. GAHJ test sample preparation

The GAHJ was obtained after filtration using a filter membrane with a 0.22- $\mu$ m pore size.

### 2.4.2. Pretreatment of plasma, urine, and bile samples

The plasma samples collected at different time after the administration were mixed. After the dilution for three times with ultrapure water, an Oasis<sup>®</sup> HLB column extractor was used for enrichment and purification. The blank plasma sample processing procedure was the same as above.

The urine and bile samples collected at 0–24 h after the administration were mixed. The Oasis<sup>®</sup> HLB column extractor was used for enrichment and purification. In addition, blank urine and rat bile samples were prepared with the same pretreatment method.

For the above samples, the methanol eluent was collected and dried with nitrogen as the drying medium, followed by redissolution using 70% methanol. The treated samples were sonicated for 10 s, vortexed, and centrifuged at 12,000 r/min for 10 min (D3024, DLAB Scientific Co., Ltd., Beijing, China) to collect the supernatant for further analysis. The sample preparation processes are detailed in Section 3 “Sample preparation” in the Supplementary data.

### 2.4.3. Pretreatment of rat fecal samples

The rat fecal samples collected at 0–24 h after the administration of GAHJ were mixed. Then, the samples were extracted with three times the amount of ultrapure water and methanol. The

sample preparation process is detailed in Section 3.6 “Pretreatment of rat fecal samples” in the Supplementary data.

## 2.5. UPLC-HRMS analysis

The sample detection was performed with a Thermo Fisher Q Exactive Orbitrap mass spectrometer (Thermo Fisher Scientific Inc., Waltham, MA, USA). Mobile phases A and B were H<sub>2</sub>O with 0.1% formic acid and 100% acetonitrile, respectively. Sample separation was performed using an ACQUITY UPLC charged-surface hybrid (CSH) C<sub>18</sub> chromatographic column (2.1 mm  $\times$  50 mm, 1.7  $\mu$ m; Waters, Milford, MA, USA) at 30  $^{\circ}$ C, and the flow rate was 0.3 mL/min. The gradients were set as follows: 0–2 min (2% B); 2–10 min (2%–10% B); 10–12.5 min (10%–15% B); 12.5–16.5 min (15%–20% B); 16.5–19.5 min (20%–30% B); 19.5–21.5 min (30%–35% B); 21.5–23.5 min (35%–95% B); 23.5–28 min (95%–95% B); 28–28.1 min (95%–2% B); 28.1–33.1 min (2% B). The eluent was monitored at the ultraviolet (UV) wavelengths of 205, 254, and 310 nm. The injection was performed at the volume of 1  $\mu$ L for GAHJ and 3  $\mu$ L for the samples.

The MS parameters were set as follows: full MS resolution of 35,000; scanning range *m/z* of 100–1200; dd-MS2 resolution of 17,500; (N) collision energy (CE)/stepped (N) CE of 35%; spray voltage (+) of 3.8 kV; spray voltage (–) of 3.5 kV; capillary temperature of 320  $^{\circ}$ C; sheath gas (N<sub>2</sub>) flow rate of 35 arb; sweep gas (N<sub>2</sub>) flow rate of 5 arb; and auxiliary gas (N<sub>2</sub>) flow rate of 10 arb.

## 2.6. Network pharmacology

In our research, high-exposure components were selected for efficacy prediction based on the identification results of related compounds in the human body after GAHJ administration. Taking the name of the compound as the keyword, the seed gene was searched in Traditional Chinese Medicine Systems Pharmacology Database and Analysis Platform (<http://tcmispw.com/tcmisp.php>) and SwissTarget Prediction (<http://www.swisstargetprediction.ch/>). The “drug–target” information table was exported with the deletion of redundant data. Furthermore, for the identification of human genes, disease-related targets were searched in the Comparative Toxicogenomics Database (<http://ctdbase.org/>) with “Pneumonia” as the keyword. Furthermore, the protein–protein interaction network (high confidence: 0.700) of co-targets was constructed in the STRING database (<https://string-db.org/cgi/input.pl>). The subsequent analysis was continued using Cytoscape\_v3.7.2 software to screen the top 100 key proteins. In the final step, molecular network analysis was carried out using Cytoscape\_v3.7.2 software and ClueGO plug-in.

## 2.7. Molecular docking

Genetic Optimization for Ligand Docking (GOLD) [26] (version 5.2), the molecular docking program released by the Cambridge Crystallographic Data Center, was used for the docking study. The crystal structures of potential targets were obtained from Protein Data Bank (PDB), and the binding sites were indicated by the original complexed ligand in each protein. Each compound was docked 10 times, starting with different random ligand orientations and using the default automatic genetic algorithm parameter settings.

## 2.8. Immunohistochemistry assay

The middle lobe of the right lung collected in the mouse model with pneumonia was fixed in 4% tissue fixative, embedded in paraffin, cut into 4  $\mu$ m-thick sections, and dewaxed for

immunohistochemical analysis. The slides were incubated with iNOS (ab15323, 1:100) and TNF- $\alpha$  (ab109322, 1:150) primary antibody overnight at 4 °C. The protein expression was determined based on the positive chromogenic markers. Low- and high-expression results were detected as yellow and brown staining, respectively. All slides were observed under a biological microscope (Olympus BX53, Olympus Corporation, Miyazaki, Japan). The detailed procedures are described in Section 4 “Immunohistochemistry assay” in the Supplementary data.

### 2.9. Measurement of iNOS and TNF- $\alpha$ in serum samples

Mouse iNOS and TNF- $\alpha$  ELISA kits were used for the detection of iNOS and TNF- $\alpha$  concentrations in the serum, respectively. A microplate reader was used to measure the absorbance at 450 nm wavelength. The concentrations of iNOS and TNF- $\alpha$  were determined by a standard curve.

### 2.10. Quantitative real-time PCR (qRT-PCR)

The experimental mice were dissected for the collection of lung tissues, which were stored at -80 °C before further use. Trizol reagent was used to extract the total RNA, and the isolated RNA was dissolved in 20  $\mu$ L of diethyl pyrocarbonate and stored at -80 °C until further use. The reaction system was 20  $\mu$ L in volume, containing 1  $\mu$ L of sample template DNA, 10  $\mu$ L of one-step Hieff<sup>®</sup> qPCR SYBR<sup>®</sup> Green Master Mix (Low Rox Plus), 10  $\mu$ M primer (0.4  $\mu$ L each), and 8.2  $\mu$ L of ultrapure water. The reaction conditions were 95 °C for 5 min (1 cycle), 95 °C for 10 s, and 60 °C for 30 s (40 cycles in total). Agilent AriaMx (Agilent Technologies Co., Ltd., Palo Alto, CA, USA) was utilized for the analysis of PCR products. The primers (Xiamen Bioray Biotechnology Co., Ltd., Fujian, China) used for qRT-PCR were as follows: glyceraldehyde-3-phosphate dehydrogenase (GAPDH) (F: CCTCCGCTGTCCTACCC; R: CAACCTGGTCCTCAGTG-TAG), iNOS (F: GGTGAAGGGACTGAGCTGTT; R: ACGTCTCCGTTCTTGACAG); and TNF- $\alpha$  (F: CTTCTCATTCTGCTT-GTG; R: ACTTGGTGGTTTGCTACG). The  $2^{-\Delta\Delta CT}$  method was used to calculate the iNOS and TNF- $\alpha$  expression levels, with GAPDH as the internal reference.

### 2.11. RAW264.7 cell culture

Mouse macrophage RAW264.7 cells were cultured in Dulbecco's modified Eagle medium (Gibco, Carlsbad, CA, USA) containing 20% fetal bovine serum and 1% penicillin-streptomycin in an incubator containing 5% CO<sub>2</sub> at 37 °C.

### 2.12. Cell viability analysis

The cytotoxicity test was achieved with the 3-(4,5-dimethylthiazol-2-yl)-2,5-diphenyltetrazolium bromide (MTT) test. Prior to the test, RAW264.7 cells were inoculated in 96-well plates at a cell density of  $1 \times 10^5$  cells/well and treated with the drug. After 24 h of incubation, the medium containing channel compounds were replaced with MTT solution for another 4 h of culture. Subsequently, 150  $\mu$ L of dimethyl sulfoxide was supplemented after removal of the culture medium in the 96-well plate. Finally, the UV absorbance at the 490 nm wavelength was measured using a microplate absorbance reader (CMax Plus, Molecular Devices, San Francisco, CA, USA).

### 2.13. Nitric oxide synthase (NOS) activity assay

RAW 264.7 cells were stimulated with 1  $\mu$ g/mL LPS [27,28] for 24 h to trigger the proinflammatory response. Other treatments,

including monomer compounds at different concentrations, were added to the cells together with LPS. The activity of NOS was detected with a NOS assay kit combined with a specific inhibitor of iNOS.

### 2.14. Western blotting (WB) assay

RAW264.7 cells ( $1 \times 10^5$  cells) were cultured in a six-well plate medium for 12 h. Afterward, the cells were treated with active monomer compounds at the specified concentration in the medium containing LPS (1  $\mu$ g/mL) for 24 h. Following washing with cooled phosphate-buffered saline (PBS), the cells in each treatment group were added with a 200  $\mu$ L of protein extraction solution containing 1% protease inhibitor.

The protein was denatured in sodium dodecyl sulfate (SDS). The samples were then subjected to SDS-PAGE, followed by transfer to the nitrocellulose membrane. Under room temperature, the cell membranes were exposed to Tris-buffered saline with 0.1% Tween<sup>®</sup> 20 (150 mM NaCl, 0.1% Tween-20, and 50 mM Tris-HCl (pH 7.5)) containing 5% skimmed milk for 1 h to inhibit nonspecific binding. Subsequently, the treated membranes were incubated with iNOS (Cat. No.: A0312, 1:1000) overnight at 4 °C. After rinsing with PBS containing 0.1% Tween-20, the membranes were incubated with anti-rabbit IgG or anti-mouse IgG coupled with horseradish peroxidase for 1 h. To visualize the protein expressions with enhanced chemiluminescence reagent, we analyzed the relative density of the bands using ImageJ software.

### 2.15. Molecular dynamic (MD) simulation

The cocrystal structure of human iNOS with inhibitor AR-C9579 (PDB ID 3E7G) was obtained [29]; AR-C9579 was used as the reference for molecular docking with GOLD, and the complex structure of glycyrrhetic acid-iNOS was obtained and used for the following MD simulation study. In the case of iNOS, two substrates, namely, protoporphyrin IX containing Fe (HEM) and 5,6,7,8-tetrahydrobiopterin (H4B), were complexed and used to determine the biological effects. H4B forms a tight H bond with the propionate of the HEM A ring and provides an electron, which is essential for activating the dioxygen combined with HEM during the catalytic reaction [30,31]. Although the binding of H4B is unnecessary for iNOS dimerization, it interacts with the two subunits of the dimer to increase the structural stability [32]. As HEM and H4B are close to the active site, they were included in the MD simulations. The Gaussian16 with B3LYP 6-31G\* basis set was used for ab-initial quantum mechanics calculations to optimize the molecular geometries of HEM, H4B, and glycyrrhetic acid, and the partial charges were calculated and fitted with the electrostatic potential with restrained electro static potential. The truncated octahedral TIP3P water box was used to explicitly solvate the system with the force field of Amber ff14SB and generalized amber force field, and sufficient ions were added to neutralize the charges of the whole system.

The energy minimizations and equilibrations that accord with our standard protocol [33] were first used to optimize the system; then, 100 ns free MD simulation with NPT ensemble (T = 300 K; P = 1 atm) was performed. The cutoff of nonbonded interaction was set as 8 Å, and particle-mesh-Ewald method and periodic boundary conditions were applied to treat the long-range electrostatic effects. Once the trajectory was stable, 100 snapshots were collected, and the normal mode and molecular mechanics Poisson-Boltzmann surface area (MM-PBSA) were used for the binding free energy calculation of glycyrrhetic acid and iNOS, and the contribution of each residue was calculated using the binding free energy decomposition.

### 3. Results

#### 3.1. UPLC-HRMS analysis of GC-related components of GAHJ

GC contains various components, and some of them share the similar structures. For the optimal separation of components in GC, the Waters ACQUITY UPLC CSH C<sub>18</sub> column was selected as the stationary phase, associated with the optimization of the mobile phase system and elution conditions. The 0.1% formic acid water (A)-100% acetonitrile (B) was the most suitable condition for LC analysis. According to the final optimized conditions, the high-resolution total ion chromatogram (TIC) of the GAHJ test sample was evaluated using UPLC-HRMS (Fig. 1). A total of 193 relevant components of GC were found in GAHJ, and their HRMS and tandem MS (MS/MS) data are provided in Table S1. Furthermore, the structures of relevant components of GC detected in GAHJ were analyzed in accordance with the search report of Compound Discoverer 3.1 software, in combination with the regular MS pattern of the reference substance and the corresponding characteristic fragment ion information. Our experiment conjectured the possible structures of 139 compounds, of which 10 (magnoflorine, liquiritin, ononin, daidzein, liquiritigenin, calycosin, formononetin, isoliquiritigenin, glycyrrhizin, and glycyrrhetic acid) were confirmed by the standard substance (Fig. S1). Meanwhile, the majority of the 139 compounds identified belonged to the categories of flavonoids and triterpenoid saponins.

#### 3.2. Recognition and identification of the GC-related components of GAHJ exposed in humans

Our research group established a comprehensive recognition and identification strategy for the exposed components of TCM in vivo using various intelligent postprocessing technologies of MS-based data [17,19,34], such as high-resolution extracted ion chromatography, precise and thorough background subtraction (PATBS), mass defect filter (MDF), data independent acquisition-product ion filter, and other targeted and nontargeted analyses. In

this study, from the perspective of exposure in humans and based on our previously developed technology strategy [17], a comprehensive identification-characterization was performed to study GC-related exposed components. Fig. 2 shows the processing results obtained by PATBS and MDF technologies. Compared with blank plasma (Fig. 2A), the unprocessed chromatogram of the human plasma sample after the GAHJ administration (Fig. 2B) showed that although several GC-related components were detected, most of the peaks were endogenous components. By contrast, the chromatograms of the same plasma samples treated with PATBS were notably simple, with considerably less interferences of endogenous components on GC components (Figs. 2C and D). In addition, PATBS technology was used for the search of in vivo components, which significantly simplified the full-scan MS datasets. For instance, the full-scan MS spectrum of the GC-relevant component (glycyrrhetic acid) showed a single molecular ion without any evident interference ion species (Fig. 2E). The mass spectral trees similarity filter (MTSF) processing tool automatically compared the mass spectral data of prototypical components and detected metabolites to associate certain metabolites, with individual prototypical components based on the mass spectral similarity. As mass defect shifts of all types of metabolites are within predictable window of the mass defect filter templates, the MDF technique was used to identify whether the GC-related components of GAHJ are possibly from the prototype components or from its precursor metabolite components. Based on the structures of metabolite components and using MTSF and MDF techniques, the correlations between GC metabolites obtained in vivo and individual prototypical components were established. Thus, the assessment of biotransformation of major GC components could be evaluated. In this study, the MDF technique was used to construct the association between the main components of GC and their related metabolites in vivo. Using the main prototype components of GC as the MDF template (Fig. 2F) and glycyrrhetic acid as the filter template, the interference of some endogenous components could be eliminated, and the transformation relationship between the exposed components of GC and its metabolites in vivo could be constructed. Therefore, the

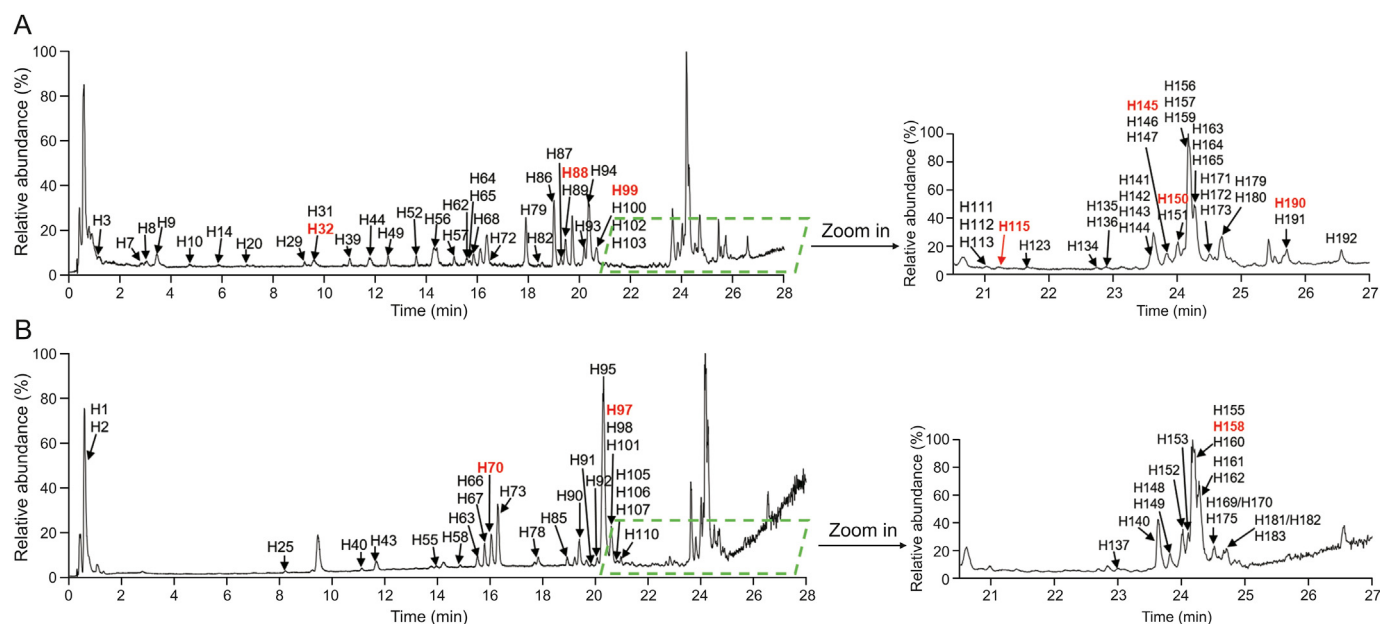


**Fig. 1.** High-resolution total ion chromatogram (TIC) of Gan An He Ji oral liquid (GAHJ) via ultra-high performance liquid chromatography-high-resolution mass spectrometry (UPLC-HRMS) analysis. (A) TIC of GAHJ in positive ion mode; (B) TIC of GAHJ in negative ion mode. The number with red font represents the compound with the reference substance identification.

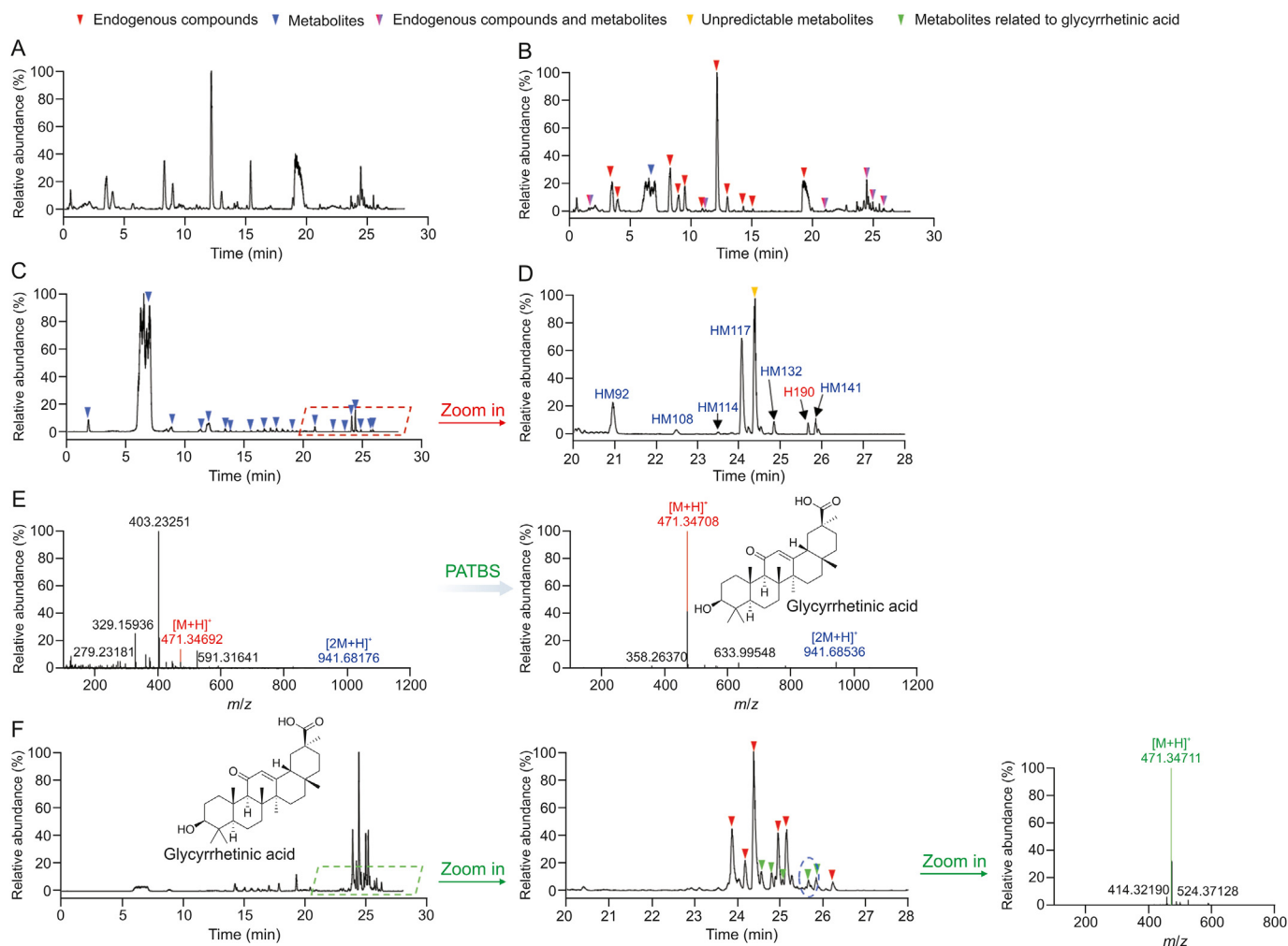


**Fig. 2.** Analysis of Gan Cao (GC) components in the human plasma samples using ultra-high performance liquid chromatography-high-resolution mass spectrometry (UPLC-HRMS) (positive ion mode) by precise and thorough background subtraction (PATBS) and mass defect filter (MDF) data processing. Chromatography of full-scan MS analysis of (A) blank human plasma samples (pre-dosed) and (B) human plasma samples. (C) PATBS-processed chromatography of full-scan MS analysis and the (D) partially enlarged view. (E) Full-scan MS spectrum of the GC component glycyrrhetic acid from PATBS-processed UPLC-HRMS dataset. (F) MDF-processed chromatography of full-scan MS analysis ( $\pm 50$  mDa).

accurate MS/MS spectral data for GC components detected in the plasma samples could be retrieved from the recorded MS/MS dataset. The structural characterization of GC-relevant components was further completed by comparing their HRMS data with reference standards, GAHJ test solutions (Fig. 1), spectral interferences, and biotransformation. According to the results, 168 related components of GC, including 24 prototypical components and 144 metabolites, were obtained in humans, with 135 compounds screened in plasma and 82 in urine.

Figs. 3A and B show the representative high-resolution TIC of GC-related components in positive and negative ion modes for human plasma and urine samples after repeated administration, respectively. Fig. 3C shows the relative ratio of the identified and unidentified components. Table S2 shows the HRMS and MS/MS data of compounds in vivo. In general, the components of TCM absorbed in vivo were probably the main active components, especially those with the high-exposure level and good pharmacokinetic characteristics. In our study, 15 relatively high-exposure components were detected among the 130 identified GC-related components discovered in vivo, as mentioned above (Fig. 3D). In the view of the metabolic transformation relationship in vivo, these highly exposed components were related to six components, namely, liquiritin (H70), liquiritigenin (H97), daidzein (H99),

formononetin (H145), glycyrrhizin (H158), and glycyrrhetic acid (H190). Among the 130 compounds identified in humans, the relative exposures of these six components and their metabolites in plasma and urine accounted for 78% and 60%, respectively (Fig. 3E). Fig. 3F presents the metabolic pathways of the six components in humans after repeated administration. Through the human exposure assessment, the six components were the main GC-related active components in vivo. Simultaneously, considering the content differences of these components in GC, for example, the concentrations of liquiritin, liquiritigenin, daidzein, formononetin, glycyrrhizin, and glycyrrhetic acid were 126.1, 12.4, 37.1, 35.5, 1103.1, and 25.1  $\mu\text{g}/\text{mL}$ , respectively. In the current experiment, a potential active-component complex composed of these six monomers was prepared for further pharmacodynamic verification.

### 3.3. Analysis of ADME metabolic profile of the GC-related components of GAHJ in rats

To deeply understand the metabolism and clearance pathways of the GC-related active components exposed in vivo and learn the metabolic differences in different species (rats and human), we made further exploration concerning the metabolic profiling of the

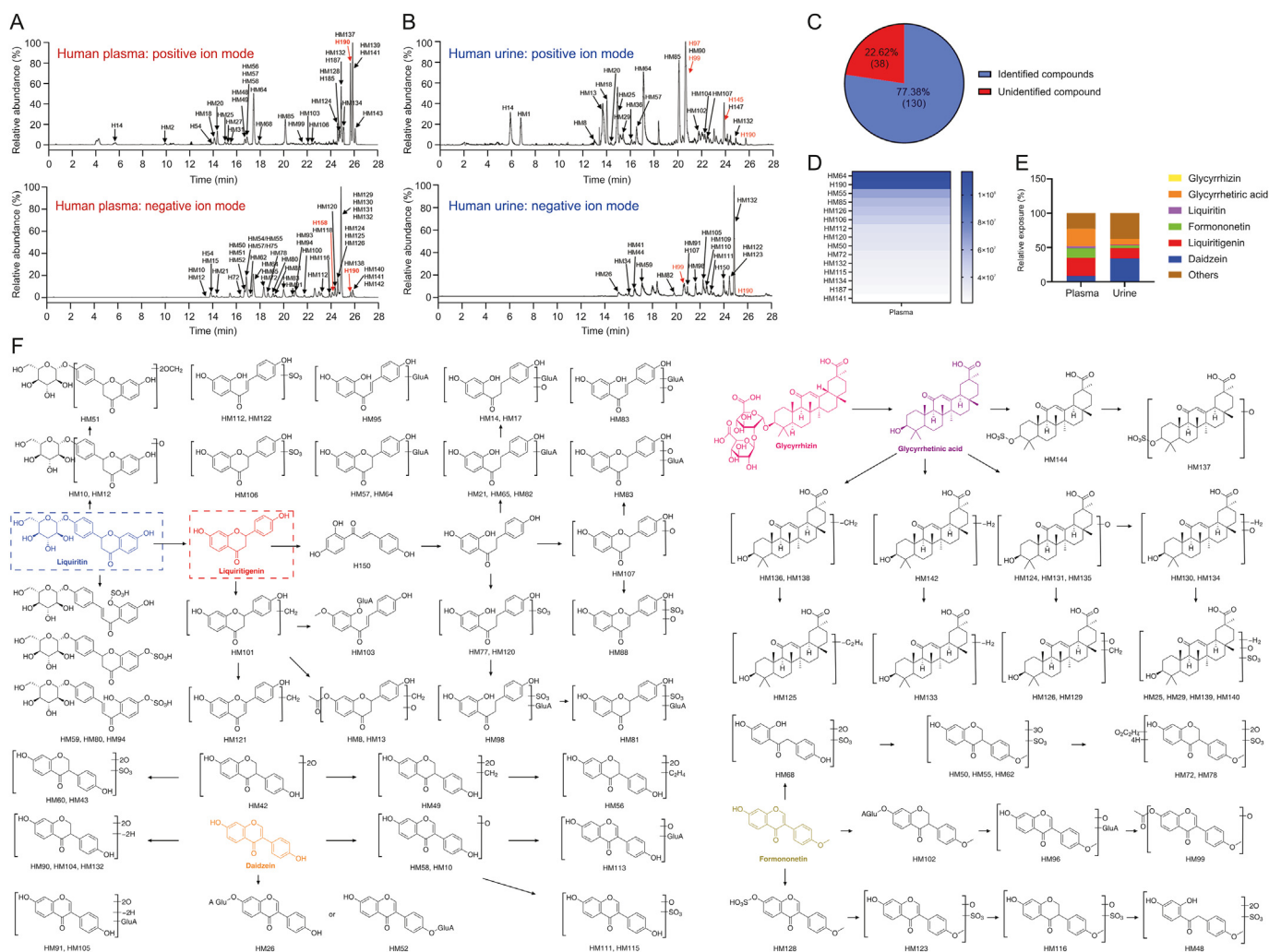


**Fig. 3.** High-resolution total ion chromatogram (TIC) of Gan Cao (GC)-related components in biological samples after the oral administration of Gan An He Ji oral liquid (GAHJ) via ultra-high performance liquid chromatography-high-resolution mass spectrometry (UPLC-HRMS) analysis. High-resolution TIC of human (A) plasma and (B) urine samples in positive and negative ion modes; (C) the relative ratio of the identified and unidentified components of GC in vivo; (D) top 15 chemical components in the plasma exposure of the 130 identified GC-related components discovered in vivo; (E) relative exposure ratio of the identified components in vivo in plasma and urine; and (F) metabolic pathways of six GC components (liquiritin, liquiritigenin, daidzein, formononetin, glycyrrhizin, and glycyrrhetic acid) in humans. The numbers in red represent the components with reference substance identification.

ADME of GC-related components in vivo after oral GAHJ administration in rats. Based on the previously developed ADME research strategy of TCM [19,34], 210 GC-related components, consisting of 86 prototype components and 124 metabolites, were found in the rats. The HRMS and MS/MS data of compounds in vivo are provided in Table S3. Specifically, 147 compounds were found in the plasma, 109 in urine, 87 in feces, and 37 in bile. Figs. 4A and B show the representative high-resolution TIC of GC-related components in positive and negative ion modes for rat plasma and urine samples after the repeated administration, respectively. Fig. S2 presents the high-resolution TIC of the fecal and bile samples. The ADME profile in vivo was constructed following the detection of GC-related components in different biological samples of rats. The flavonoids in GC, which are excreted primarily in the form of glucuronidation, may undergo sulfation, oxidation, glucuronidation, methylation, and other reactions in vivo (Fig. 4C). Meanwhile, the demethylation, sulfation, and glycoside removal are the predominant metabolic pathways of triterpenoids in vivo, with the removal of glycoside metabolites as the primary approach for excreting triterpenoids out of the body (Fig. 4D). Collectively, these findings indicated the good

similarity of GC-related components detected in rats after oral GAHJ administration and those tested in patients with pneumonia, which may ensure the reliability of subsequent pharmacodynamic experiments in rats.

#### 3.4. Network pharmacology and molecular docking of the GC-related active components

The compound-disease-target network was constructed by integrating potential GC-related active components with 100 key targets of pneumonia, involving 50 common targets shared by the six primary components in total. Subsequently, the screened 50 targets were selected for Kyoto Encyclopedia of Genes and Genomes (KEGG) pathway and Gene Ontology enrichment analyses. KEGG pathway analysis showed that the majority of the 50 key proteins were associated with inflammatory and pneumonia-related pathways, such as mitogen-activated protein kinase signaling pathway (Fig. 5). Based on the results of network pharmacology, common targets with a degree >4 (12 proteins in total) were selected, and the molecular docking studies were performed

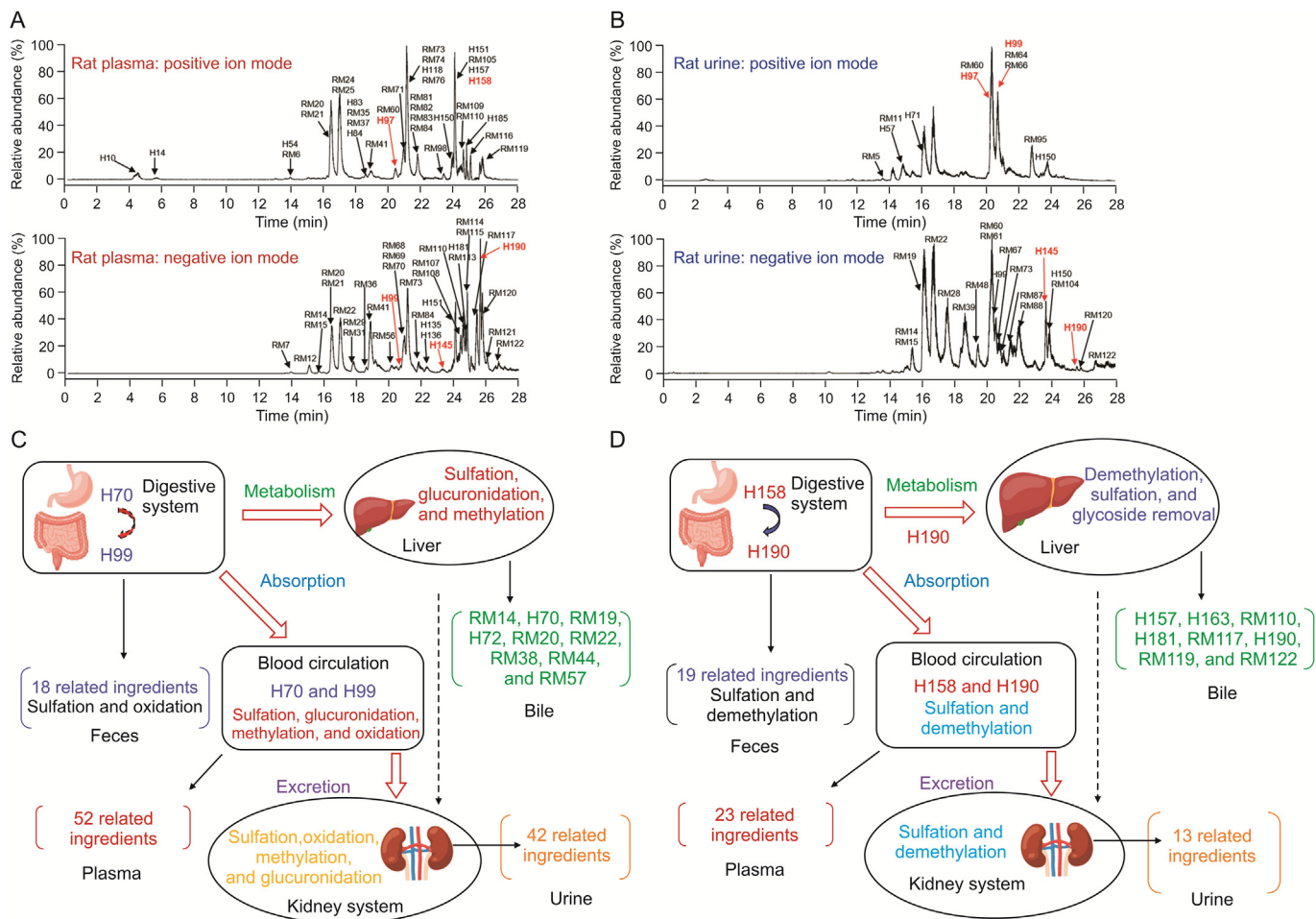


**Fig. 4.** The absorption, distribution, metabolism, excretion (ADME) metabolic profile of typical components of Gan Cao (GC) exposed in rats in vivo. High-resolution total ion chromatogram of rat (A) plasma and (B) urine samples in positive and negative ion modes. The numbers in red represent the components with reference substance identification. (C) ADME profile of flavonoids in GC in rats, including typical biotransformation reactions (with liquiritin and liquiritigenin as examples); (D) ADME profile, including typical biotransformation reactions (with glycyrrhizin and glycyrrhetic acid as examples), of triterpenoids in GC in rats.

on 10 of them, whose crystal structures were solved and available in the PDB. The molecular docking scores (Table S4) indicated that iNOS was ranked with the highest score for compounds

liquiritigenin, glycyrrhetic acid, daidzein, and formononetin. In general, iNOS is a messenger molecule with diverse functions throughout the body, and it is responsible for the production of

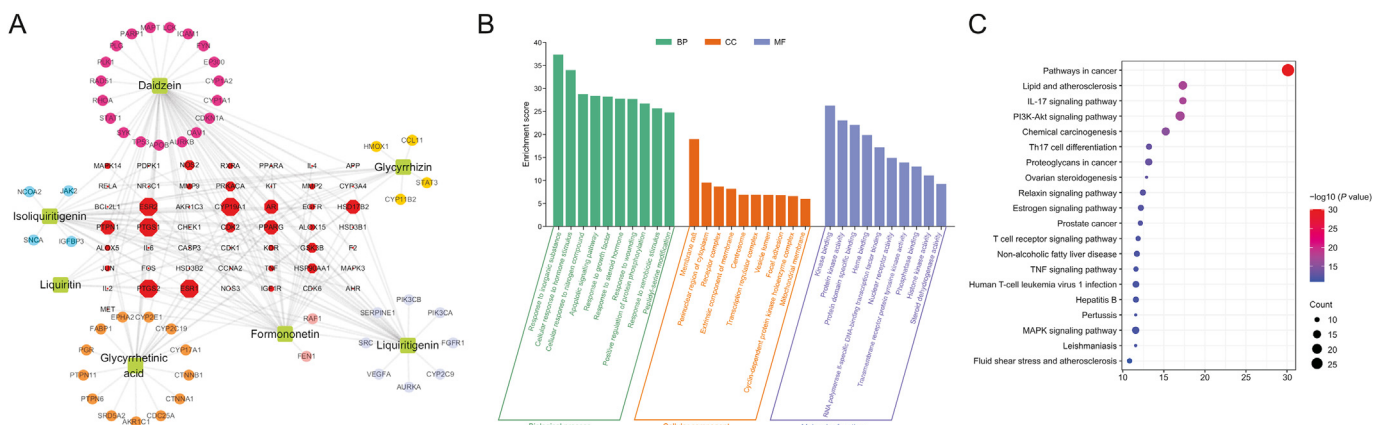


**Fig. 5.** Construction of potential active component-key target network and gene ontology (GO) and Kyoto Encyclopedia of Genes and Genomes (KEGG) pathway enrichment analysis. (A) Drug-target network constructed using the potentially active components of Gan An He Ji oral liquid (GAHJ) and 100 key proteins; (B) top 30 GO terms with  $P < 0.01$ ; (C) top 20 pathways with  $P < 0.05$ . BP: biological processes; CC: cellular components; MF: molecular functions; IL: interleukin; PI3K-Akt: phosphatidylinositol 3-kinase-protein kinase; Th17: T helper 17; TNF: tumor necrosis factor; MAPK: mitogen-activated protein kinase.

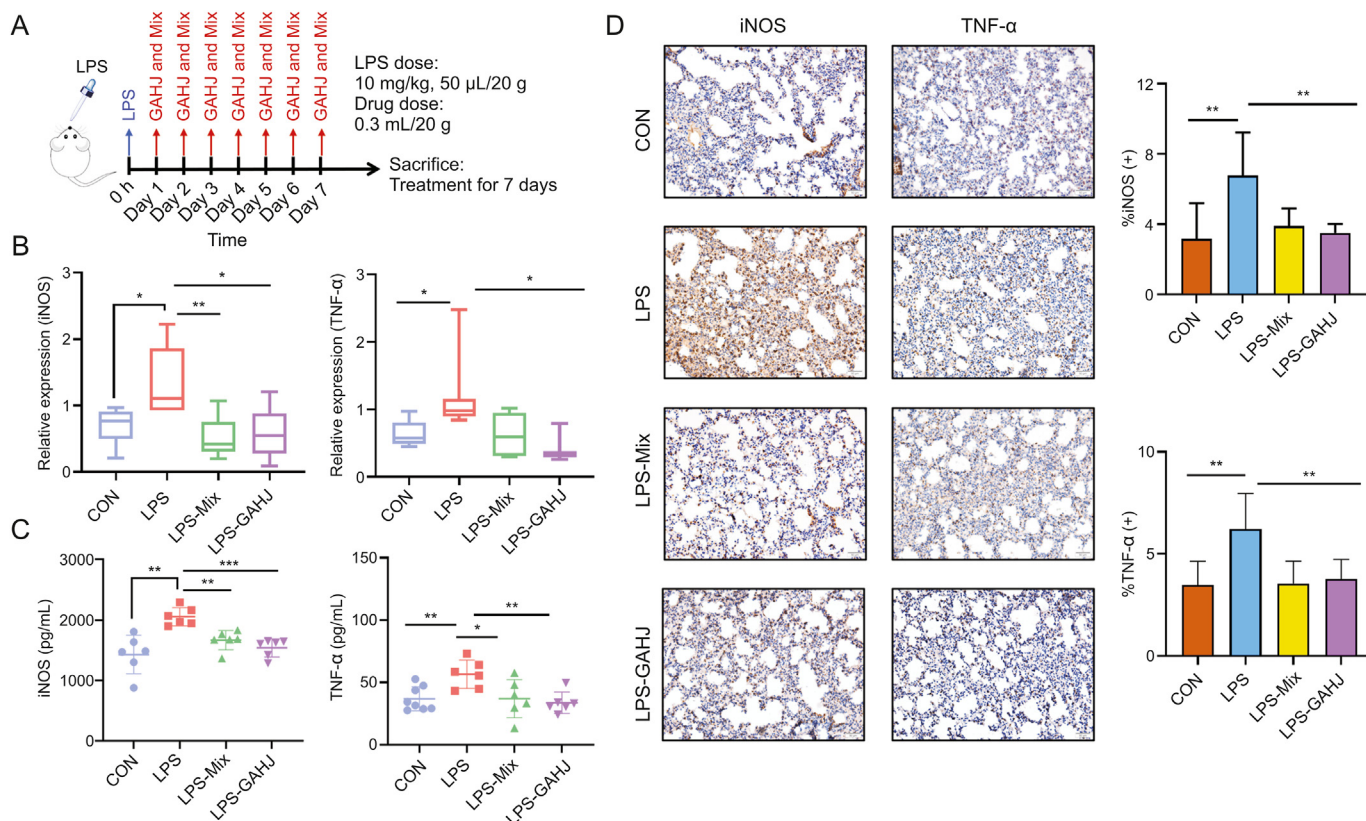


**Fig. 6.** Potentially active components, which were screened from the perspective of in vivo exposure in patients with pneumonia, can significantly downregulate inducible nitric oxide synthase (iNOS) and reduce the level of lung inflammation. (A) Schematic of lipopolysaccharide (LPS)-induced animal model of pneumonia; (B) mRNA expressions of iNOS and tumor necrosis factor (TNF)- $\alpha$  in the lung tissues from the control (CON), LPS, LPS-Mix, and LPS-Gan An He Ji oral liquid (GAHJ) groups identified by quantitative real-time polymerase chain reaction ( $n = 6$ ); (C) expression levels of iNOS and TNF- $\alpha$  in plasma from the CON, LPS, LPS-Mix, and LPS-GAHJ groups by determined by enzyme-linked immunosorbent assay ( $n = 6$ ); (D) immunohistochemical assay results of iNOS and TNF- $\alpha$  in lung tissues from the CON, LPS, LPS-Mix, and LPS-GAHJ groups (scale: 50  $\mu$ m). (B–D) Data are expressed as mean  $\pm$  standard error of the mean ( $n = 6$ , the analysis of variance). \* $P < 0.05$ , \*\* $P < 0.01$ , and \*\*\* $P < 0.001$ .

nitric oxide (NO) [35,36]. iNOS can participate in the inflammatory response in vivo and enhance the synthesis of proinflammatory mediators, such as interleukin (IL)-6 and IL-8 [37]. Furthermore, high levels of NO, superoxide, and other inflammatory products derived from iNOS can induce hemodynamic collapse in vivo, which is manifested as impaired vascular permeability, vasodilation, insufficient tissue perfusion, and intractable hypotension [38]. In this regard, the identification of iNOS inhibitors is significant in inhibiting cytokine storm and alleviating inflammatory symptoms, thus providing a feasible approach for the treatment of pneumonia. On the basis of network pharmacology and molecular docking data, iNOS was screened as a potential target protein for further validation of pharmacodynamic mechanism of GC-related components.

### 3.5. Efficacy verification of GC-related components in a mouse model of LPS-induced pneumonia

The therapeutic effect of potential GC-related active-component complex on the LPS-induced mouse model of pneumonia was further verified, in association with the validation of its regulatory effect on the potential target iNOS. Fig. 6A shows the schematic of the LPS-induced mouse model of pneumonia. According to the detection results of qRT-PCR, the mRNA level of iNOS in the LPS group significantly increased with respect to that in the CON group, and such increment was significantly eliminated in the LPS-Mix and LPS-GAHJ groups (Fig. 6B). The results of ELISA were

consistent with those of the PCR (Fig. 6C). The level of iNOS returned to normal after treatment with potential active-component complex and GAHJ. Furthermore, based on the immunohistochemical assay results of the lung tissues (Fig. 6D), similar trends were observed when using ImageJ software to analyze the iNOS-positive area. In the LPS group, the iNOS antigen increased significantly in the lungs, but was evidently downregulated in the LPS-Mix and LPS-GAHJ groups. The above results suggested that the potential active-component complex could significantly downregulate the expression of iNOS, which may exert effects in treating pulmonary inflammation and improving pulmonary functions.

### 3.6. Efficacy verification of GC-related components in a mouse model of *S. Aureus*-induced pneumonia

In addition to the LPS-induced mouse model of pneumonia, another mouse model of *S. aureus*-induced pneumonia was constructed to further validate the regulation of GC-related active components on iNOS. Fig. 7A shows the schematic of modeling. The same regulation outcomes as those in the LPS-induced model accorded with the results of qRT-PCR, ELISA, and immunohistochemical assay. Specifically, the expression of iNOS in the model group (*S. aureus* group) was highly upregulated compared with that in the normal lung tissue (CON group), and it was substantially lower in the *S. aureus*-Mix and *S. aureus*-GAHJ groups than in the *S. aureus* group, whose level was almost reduced to that in the CON group (Figs. 7B–D). Consequently, the verifications with two different pneumonia models confirmed that the screened active

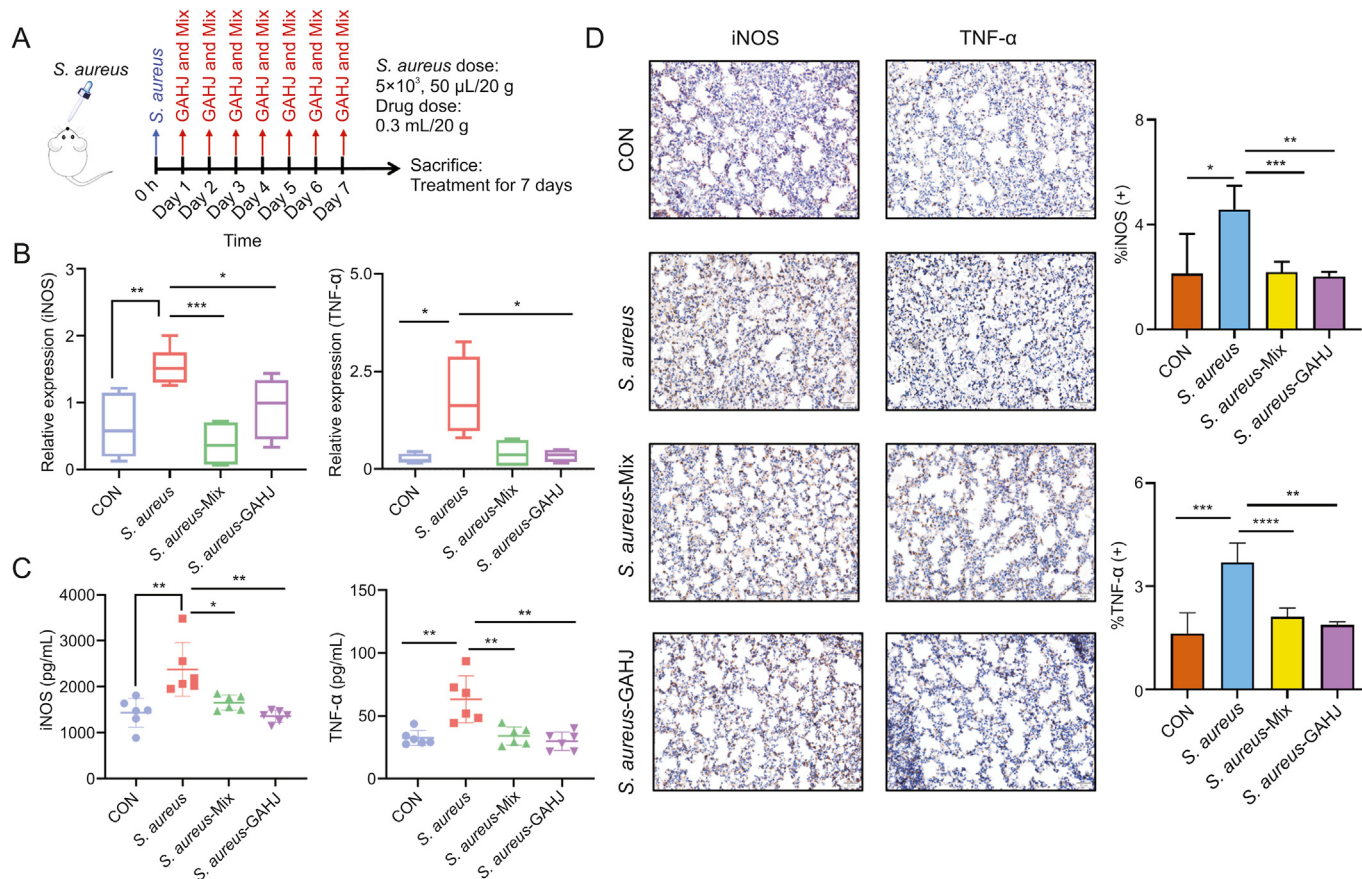


**Fig. 7.** Potentially active components, which were screened from the perspective of in vivo exposure in patients with pneumonia, could also downregulate inducible nitric oxide synthase (iNOS) and reduce the level of lung inflammation in the mouse model of *Staphylococcus aureus* (*S. aureus*)-induced pneumonia. (A) Schematic of animal pneumonia model induced by *S. aureus*; (B) mRNA expressions of iNOS and tumor necrosis factor (TNF)- $\alpha$  in lung tissues from the control (CON), *S. aureus*, *S. aureus*-Mix, and *S. aureus*-Gan An He Ji oral liquid (GAHJ) groups detected by quantitative real-time polymerase chain reaction ( $n = 6$ ); (C) expression levels of iNOS and TNF- $\alpha$  in plasma from the CON, *S. aureus*, *S. aureus*-Mix and *S. aureus*-GAHJ groups determined by enzyme-linked immunosorbent assay ( $n = 6$ ); (D) immunohistochemical assay results of iNOS and TNF- $\alpha$  in lung tissues from the CON, *S. aureus*, *S. aureus*-Mix, and *S. aureus*-GAHJ groups (scale: 50  $\mu$ m). (B–D) Data are expressed as mean  $\pm$  standard error of the mean ( $n = 6$ , the analysis of variance). \* $P < 0.05$ , \*\* $P < 0.01$ , \*\*\* $P < 0.001$ , and \*\*\*\* $P < 0.0001$ .

components could significantly downregulate the expression of iNOS, revealing a good pharmacological effect on the alleviation of pulmonary inflammation and function. Our study identified for the first time the GC-related active components, and their complex exerted similar effects as GAHJ in the treatment of pneumonia.

### 3.7. Inhibitory effect of six active components of GC on iNOS at the cellular level and in MD simulation

The inhibitory effects of the six active GC components on iNOS were further verified at the cellular level. Fig. 8B shows the cytotoxicity test results for each component. The half maximal inhibitory concentration values (glycyrrhetic acid: 45.53  $\mu$ M; liquiritin: 2609.74  $\mu$ M; daidzein: 1161.04  $\mu$ M; liquiritigenin: 499.53  $\mu$ M; glycyrrhizin: 1138.25  $\mu$ M; and formononetin: 397.54  $\mu$ M) were calculated to determine the appropriate concentration for the subsequent WB analysis and NOS activity detection. The results of WB (Fig. 8C) showed that 1400W [39] (a known iNOS specific inhibitor, 10  $\mu$ M), liquiritin (50  $\mu$ M), liquiritigenin (50  $\mu$ M), daidzein (12.5  $\mu$ M), formononetin (5  $\mu$ M), glycyrrhizin (12.5  $\mu$ M), and glycyrrhetic acid (10  $\mu$ M) all presented significant inhibitory effects on the protein expression of iNOS (the original image of the WB result is shown in Fig. S3). Meanwhile, the NOS enzyme activity test (Fig. 8D) indicated that glycyrrhetic acid exhibited stable inhibitory effects at three

different concentrations. At the concentration of 20  $\mu$ M, the inhibitory effect of glycyrrhetic acid was significantly superior to that of the other five compounds. To determine the interactions of glycyrrhetic acid with iNOS, we performed 100 ns MD simulation. During the full simulation, glycyrrhetic acid remained stable at the binding site, and no major conformational changes were observed in either protein or ligand, which indicated that glycyrrhetic acid could stably bind to iNOS. The MM-PBSA and normal mode methods were used to calculate the binding free energy as  $-17.74$  kcal/mol, which indicated a strong binding between glycyrrhetic acid and iNOS. The free energy distribution was analyzed, and the residues whose contributions were greater than  $-0.5$  kcal/mol were recorded (Fig. 8E). Glycyrrhetic acid formed three hydrogen bonds with Gly371, Pro350, and Val352. Met355, Ala262, Phe369, Trp463, and HEM formed strong van der Waals interactions with glycyrrhetic acid.

## 4. Discussion

TCM has been widely practiced in China for over 2000 years and has been recognized as the essence of the traditional Chinese pharmaceutical system. Understanding the material basis and mechanism of TCM has attracted great interests from the fields of drug research and development to clinical therapies. The most difficult task in the research of TCM is its complexity, which can be

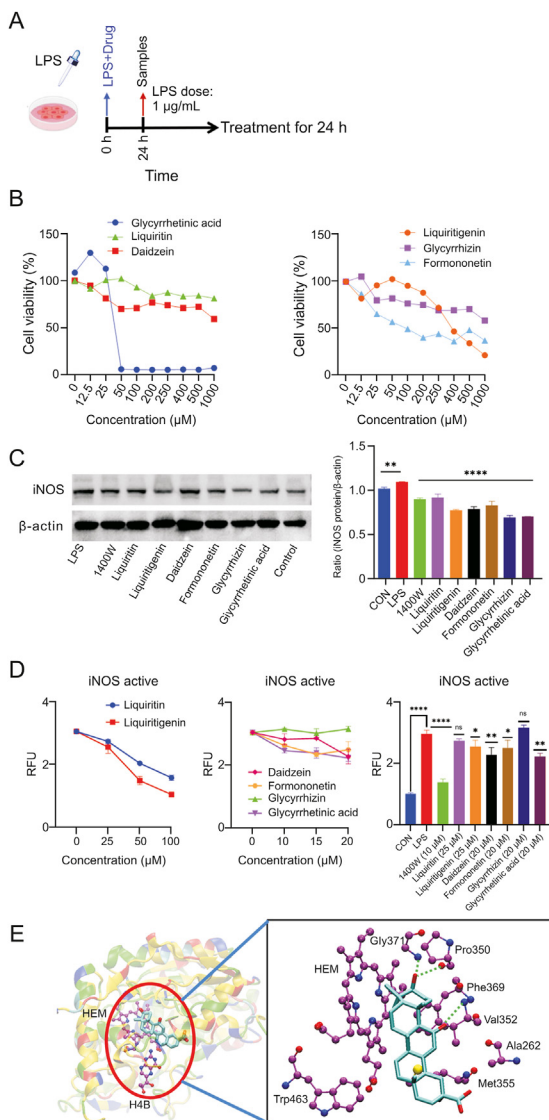


**Fig. 8.** Efficacy verification of single active components in RAW264.7 cells. (A) Schematic of lipopolysaccharide (LPS)-induced RAW264.7 cell model; (B) cytotoxicity test results of six monomers on RAW264.7 cells ( $n = 6$ ); (C) Western blotting results of inducible nitric oxide synthase (iNOS) protein inhibition by 1400W and six monomers; (D) test results of the effect of 1400W and six monomers on the nitric oxide synthase activity ( $n = 2$ ). (C and D) Data are expressed as mean  $\pm$  standard error of the mean.  $^*P < 0.05$ ,  $^{**}P < 0.01$ ,  $^{***}P < 0.001$ , and  $^{****}P < 0.0001$ ; (E) molecular dynamic simulation of glycyrrhetic acid. CON: control; RFU: relative fluorescence unit; HEM: protoporphyrin IX containing Fe.

treated as a collection of hundreds of chemical agents. Therefore, the understanding of TCM may benefit from the simplification of the substance composition of TCM to a certain extent through the removal of inactive components. In this regard, the current study successfully established a workflow to screen GC-related active components for the treatment of pneumonia and determined their possible biological targets from the perspective of exposure in clinical patients. In addition, in the current study, using the non-targeted PATBS technology, we identified the GC-related components of GAHJ and with the use of the MDF technology, constructed the association between components, which were the key steps in the whole experiment. Traditionally, MTSF and MDF technologies are mainly used to find metabolites. However, in the current study,

they were mainly applied to construct the transformation relationship between the main components and their related metabolites. The combined use of intelligent MS data mining technology, including PATBS, MDF, and MTSF, significantly increased the efficiency on the search, identification, and analysis of the related components of GAHJ *in vivo*.

The study established a five-step workflow. In the first step, the components of the GAHJ solution were recognized and identified by UPLC-HRMS. A total of 193 GC-related chemical components were identified. Among them, 139 compounds with corresponding possible structures were identified, and 10 were confirmed by reference standards, providing basic structural information for subsequent *in vivo* studies. Second, by integrating UPLC-HRMS with numerous intelligent postprocessing technologies of MS-based data, the GC-related components were identified and characterized in patients with pneumonia. Consequently, 168 GC-related active components were obtained in humans, and the biotransformation relationship among them was established simultaneously. Meanwhile, in the view of exposure in humans, six potentially active components, namely, liquiritin, liquiritigenin, daidzein, formononetin, glycyrrhizin, and glycyrrhetic acid, together with their mixture complex, were selected for the prevention and treatment of pneumonia study. In addition, further analysis was performed on the whole process of ADME in rats, resulting in the discovery of 210 GC-related components, consisting of 86 prototype components and 124 metabolites. Moreover, this part of the research realized an in-depth understanding of the metabolic clearance process of typical compounds exposed *in vivo* and determined significant metabolic differences between animals and humans. Third, network pharmacology and molecular docking were utilized to identify the potential target protein, iNOS. Fourth, the relevant animal models of pneumonia were constructed to validate the therapeutic effect of the potential GC-related active components on pneumonia and the regulation of target protein iNOS. In the final step, the regulation of each active component on the target protein was verified at the cellular level, with the identification of an optimal pharmacodynamic effect in glycyrrhetic acid. On this basis, the MD simulation was performed on the glycyrrhetic acid and iNOS complex to determine the binding free energy and detailed interactions. NO is an important mediator overproduced as an immunomodulator and additional host defense mechanism in most inflammatory and infection conditions. The increase in NO during inflammatory immune activation and infection mainly occurs due to the induction of iNOS in various cell types [40]. In the respiratory tract, the main cells expressing iNOS are alveolar epithelial and bronchial cells, infiltrating leukocytes and alveolar macrophages. Therefore, the inhibitory effect on iNOS relieves the lung inflammation and improves the lung function [41].

In the current study, we demonstrated that the main components of GC (especially glycyrrhetic acid) exhibit significant anti-inflammatory effects, and their metabolites may perform the same function. Notably, the search of new drugs from metabolites is one of the important ways in drug discovery studies. However, in the current research, given the limitations of LC-MS in the identification of metabolites, most metabolites were unavailable with the controls for *in vitro* and *in vivo* validation studies. We carefully reviewed the chemical structures of the identified metabolites, especially those of glycyrrhetic acid, and observed that sulfation, oxidation, and demethylation are the main reactions *in vivo*. Based on the chemical structural similarities, they can show similar anti-inflammatory effects as their prototype components. However, to confirm this assumption, scientists should introduce medicinal chemistry studies for the chemical synthesis of these metabolites,

and for novel drug discovery, structural optimizations can be performed to improve their activities and druggabilities, which will be included in our future research plan.

## 5. Conclusions

In conclusion, UPLC-HRMS technology was used to comprehensively study the exposure and metabolism of GC *in vivo*, and intelligent MS postprocessing technologies, such as PATBS, MDF, and MTSF, were used to improve the identification efficiency of TCM complex components *in vivo*. In addition, from the perspective of *in vivo* exposure in patients with pneumonia, six GC-related active components (liquiritin, liquiritigenin, daidzein, formononetin, glycyrrhizin, and glycyrrhetic acid) were screened successfully for the treatment of pneumonia. For the first time, our study disclosed that iNOS may be an essential target protein for GC-related components to exert anti-pneumonia effects. Simultaneously, validations were performed using the animal models of pneumonia, which, at the cellular level, confirmed the roles of GC in alleviating inflammation and function by regulating iNOS. Furthermore, among the six active components, glycyrrhetic acid is the most effective regulator and the component with the highest exposure in humans. To the best of our knowledge, our study is the first report on the exposure of patients with pneumonia to GC-related components. The findings of this study provide a strong evidence to identify the active components and reveal the possible corresponding mechanisms in the treatment of pneumonia, thus offering data support for the application of GC in the prevention or treatment of pneumonia.

## CRedit author statement

**Xiaojuan Jiang:** Writing - Original draft preparation, Reviewing and Editing, Conceptualization, Methodology; **Yihua Lin:** Funding acquisition, Resources, Writing - Reviewing and Editing; **Yunlong Wu:** Writing - Original draft preparation, Reviewing and Editing; **Caixia Yuan, Xuli Lang,** and **Jiayun Chen:** Data curation, Writing - Reviewing and Editing; **Chunyan Zhu:** Validation; **Xinyi Yang** and **Yu Huang:** Formal analysis; **Hao Wang** and **Caisheng Wu:** Writing - Original draft preparation, Conceptualization, Methodology, Funding acquisition.

## Declaration of competing interest

The authors declare that there are no conflicts of interest.

## Acknowledgments

This research was funded by the National Natural Science Foundation of China (Grant Nos.: 82141215, 82173694, 82173779, 82222068, and U1903119), Fujian Province Science and Technology Project (Grant Nos.: 2021J011340 and 2020Y0013), and Xiamen Municipal Bureau of Science and Technology Planning Project (Grant No.: 350222021YJ11).

## Appendix A. Supplementary data

Supplementary data to this article can be found online at <https://doi.org/10.1016/j.jpha.2022.07.004>.

## References

- [1] H. Liu, J. Wang, W. Zhou, et al., Systems approaches and polypharmacology for drug discovery from herbal medicines: An example using licorice, *J. Ethnopharmacol.* 146 (2013) 773–793.
- [2] H.-X. Sun, H.-J. Pan, Immunological adjuvant effect of *Glycyrrhiza uralensis* saponins on the immune responses to ovalbumin in mice, *Vaccine* 24 (2006) 1914–1920.
- [3] M. Jiang, S. Zhao, S. Yang, et al., An “essential herbal medicine”-licorice: A review of phytochemicals and its effects in combination preparations, *J. Ethnopharmacol.* 249 (2020), 112439.
- [4] L. Wang, R. Yang, B. Yuan, et al., The antiviral and antimicrobial activities of licorice, a widely-used Chinese herb, *Acta Pharm. Sin. B* 5 (2015) 310–315.
- [5] Y. Wang, X. Zhang, X. Ma, et al., Study on the kinetic model, thermodynamic and physicochemical properties of Glycyrrhiza polysaccharide by ultrasonic assisted extraction, *Ultrason. Sonochem.* 51 (2019) 249–257.
- [6] R. Yang, L.Q. Wang, B.C. Yuan, et al., The pharmacological activities of licorice, *Planta Med.* 81 (2015) 1654–1669.
- [7] J.Y. Yu, J.Y. Ha, K.M. Kim, et al., Anti-inflammatory activities of licorice extract and its active compounds, glycyrrhizic acid, liquiritin and liquiritigenin, in BV2 cells and mice liver, *Molecules* 20 (2015) 13041–13054.
- [8] M. Ramalingam, H. Kim, Y. Lee, et al., Phytochemical and pharmacological role of liquiritigenin and isoliquiritigenin from *Radix glycyrrhizae* in human health and disease models, *Front. Aging Neurosci.* 10 (2018), 348.
- [9] S. Pandit, S. Ponnusankar, A. Bandyopadhyay, et al., Exploring the possible metabolism mediated interaction of *Glycyrrhiza glabra* extract with CYP3A4 and CYP2D6, *Phytother. Res.* 25 (2011) 1429–1434.
- [10] T. Fukai, A. Marumo, K. Kaitou, et al., Anti-*Helicobacter pylori* flavonoids from licorice extract, *Life Sci.* 71 (2002) 1449–1463.
- [11] J. Reuter, I. Merfort, C.M. Schempp, Botanicals in dermatology: An evidence-based review, *Am. J. Clin. Dermatol.* 11 (2010) 247–267.
- [12] L. Luo, J. Jiang, C. Wang, et al., Analysis on herbal medicines utilized for treatment of COVID-19, *Acta Pharm. Sin. B* 10 (2020) 1192–1204.
- [13] Y. Xian, J. Zhang, Z. Bian, et al., Bioactive natural compounds against human coronaviruses: A review and perspective, *Acta Pharm. Sin. B* 10 (2020) 1163–1174.
- [14] J. Zhao, S. Tian, D. Lu, et al., Systems pharmacological study illustrates the immune regulation, anti-infection, anti-inflammation, and multi-organ protection mechanism of Qing-Fei-Pai-Du decoction in the treatment of COVID-19, *Phytomedicine* 85 (2021), 153315.
- [15] J. Liu, W. Yang, Y. Liu, et al., Combination of Hua Shi Bai Du granule (Q-14) and standard care in the treatment of patients with coronavirus disease 2019 (COVID-19): A single-center, open-label, randomized controlled trial, *Phyto-medicine* 91 (2021), 153671.
- [16] Y.-F. Huang, C. Bai, F. He, et al., Review on the potential action mechanisms of Chinese medicines in treating coronavirus disease 2019 (COVID-19), *Pharmacol. Res.* 158 (2020), 104939.
- [17] X. Chen, Y. Wu, C. Chen, et al., Identifying potential anti-COVID-19 pharmacological components of traditional Chinese medicine Lianhuaqingwen capsule based on human exposure and ACE2 biochromatography screening, *Acta Pharm. Sin. B* 11 (2021) 222–236.
- [18] L. van de Sand, M. Bormann, M. Alt, et al., Glycyrrhizin effectively inhibits SARS-CoV-2 replication by inhibiting the viral main protease, *Viruses* 13 (2021), 609.
- [19] C. Zhu, T. Cai, Y. Jin, et al., Artificial intelligence and network pharmacology based investigation of pharmacological mechanism and substance basis of Xiaokewan in treating diabetes, *Pharmacol. Res.* 159 (2020), 104935.
- [20] X. Wang, A. Zhang, X. Zhou, et al., An integrated chinmedomics strategy for discovery of effective constituents from traditional herbal medicine, *Sci. Rep.* 6 (2016), 18997.
- [21] T. Chen, X. Wang, P. Chen, et al., Chemical components analysis and *in vivo* metabolite profiling of Jian'er Xiaoshi oral liquid by UHPLC-Q-TOF-MS/MS, *J. Pharm. Biomed. Anal.* 211 (2022), 114629.
- [22] W. Dong, P. Wang, X. Meng, et al., Ultra-performance liquid chromatography-high-definition mass spectrometry analysis of constituents in the root of *Radix Stemonae* and those absorbed in blood after oral administration of the extract of the crude drug, *Phytochem. Anal.* 23 (2012) 657–667.
- [23] J. Shi, H. Wang, J. Liu, et al., Ganoderic acid B attenuates LPS-induced lung injury, *Int. Immunopharmacol.* 88 (2020), 106990.
- [24] Q. Wu, H. Li, J. Qiu, et al., Betulin protects mice from bacterial pneumonia and acute lung injury, *Microb. Pathog.* 75 (2014) 21–28.
- [25] R. Kapetanovic, G. Jouvion, C. Fitting, et al., Contribution of NOD2 to lung inflammation during *Staphylococcus aureus*-induced pneumonia, *Microb. Infect.* 12 (2010) 759–767.
- [26] G. Jones, P. Willett, R.C. Glen, et al., Development and validation of a genetic algorithm for flexible docking, *J. Mol. Biol.* 267 (1997) 727–748.
- [27] H.J. Yoon, M.E. Moon, H.S. Park, et al., Chitosan oligosaccharide (COS) inhibits LPS-induced inflammatory effects in RAW 264.7 macrophage cells, *Biochem. Biophys. Res. Commun.* 358 (2007) 954–959.
- [28] S.J. Hwang, Y.W. Kim, Y. Park, et al., Anti-inflammatory effects of chlorogenic acid in lipopolysaccharide-stimulated RAW 264.7 cells, *Inflamm. Res.* 63 (2014) 81–90.
- [29] E.D. Garcin, A.S. Arvai, R.J. Rosenfeld, et al., Anchored plasticity opens doors for selective inhibitor design in nitric oxide synthase, *Nat. Chem. Biol.* 4 (2008) 700–707.
- [30] S. Kang, W. Tang, H. Li, et al., Nitric oxide synthase inhibitors that interact with both heme propionate and tetrahydrobiopterin show high isoform selectivity, *J. Med. Chem.* 57 (2014) 4382–4396.
- [31] P.J. Kolodziejski, M.B. Rashid, N.T. Eissa, Intracellular formation of “undisruptable” dimers of inducible nitric oxide synthase, *Proc. Natl. Acad. Sci. U S A*

- 100 (2003) 14263–14268.
- [32] J.M. Perry, M.A. Marletta, Effects of transition metals on nitric oxide synthase catalysis, *Proc. Natl. Acad. Sci. U S A* 95 (1998) 11101–11106.
- [33] W. Hong, Y. Wang, Z. Chang, et al., The identification of novel *Mycobacterium tuberculosis* DHFR inhibitors and the investigation of their binding preferences by using molecular modelling, *Sci. Rep.* 5 (2015), 15328.
- [34] C. Wu, H. Zhang, C. Wang, et al., An integrated approach for studying exposure, metabolism, and disposition of multiple component herbal medicines using high-resolution mass spectrometry and multiple data processing tools, *Drug Metab. Dispos.* 44 (2016) 800–808.
- [35] T.J. Gross, K. Kremens, L.S. Powers, et al., Epigenetic silencing of the human NOS2 gene: Rethinking the role of nitric oxide in human macrophage inflammatory responses, *J. Immunol.* 192 (2014) 2326–2338.
- [36] X. Wang, Z. Gray, J. Willette-Brown, et al., Macrophage inducible nitric oxide synthase circulates inflammation and promotes lung carcinogenesis, *Cell Death Discov.* 4 (2018), 46.
- [37] K. Vuolteenaho, A. Koskinen, M. Kukkonen, et al., Leptin enhances synthesis of proinflammatory mediators in human osteoarthritic cartilage – mediator role of NO in leptin-induced PGE<sub>2</sub>, IL-6, and IL-8 production, *Mediators Inflamm.* 2009 (2009), 345838.
- [38] E.L. Feitosa, F.T.D.S. Júnior, J.A.O. Nery Neto, et al., COVID-19: Rational discovery of the therapeutic potential of Melatonin as a SARS-CoV-2 main protease inhibitor, *Int. J. Med. Sci.* 17 (2020) 2133–2146.
- [39] Q. Tang, C.I. Svensson, B. Fitzsimmons, et al., Inhibition of spinal constitutive NOS-2 by 1400W attenuates tissue injury and inflammation-induced hyperalgesia and spinal p38 activation, *Eur. J. Neurosci.* 25 (2007) 2964–2972.
- [40] J.W. Coleman, Nitric oxide in immunity and inflammation, *Int. Immunopharmacol.* 1 (2001) 1397–1406.
- [41] T. Okamoto, K. Gohil, E.I. Finkelstein, et al., Multiple contributing roles for NOS2 in LPS-induced acute airway inflammation in mice, *Am. J. Physiol. Lung Cell. Mol. Physiol.* 286 (2004) L198–L209.